International Journal of Control and Automation
Vol.8, No.12 (2015), pp.207-216
http://dx.doi.org/10.14257/ijca.2015.8.12.19

Numerical Simulation of Force Suppression for Flow Circular Cylinder at Low Reynolds Number

Zhendong Cui[1,2,3], Shenming Gu[1,2] and Xiwu Gong[3]

[1]*School of Mathematics, Physics & Information Science, Zhejiang Ocean University, Zhoushan, 316022, PR China*
[2]*Key Laboratory of Oceanographic Big Data Mining & Application of Zhejiang Province, Zhoushan, Zhejiang 316022, PR China*
[3]*Key Laboratory of Offshore Engineering Technology of Zhejiang Province, Zhoushan, Zhejiang 316022, PR China*
cuizd@zjou.edu.cn

Abstract

Numerical simulation was conducted for fluid flow past a circular cylinder with triangular control rod in the upstream at low Reynolds numbers. The study focuses on the influences of leg length of rod $\boldsymbol{L}$*, rod-to-cylinder spacing ratio* $\boldsymbol{S}$*, vertex angle of triangular* $\boldsymbol{\alpha}$ *of rod on the vortex shedding and forces. The results show the equilateral triangle rod in the upstream takes effective suppression of not only the lift but also the drag in the range of* $0.2\boldsymbol{R} \leq \boldsymbol{L} \leq 0.5\boldsymbol{R}$ *and* $3\boldsymbol{R} \leq \boldsymbol{S} \leq 6\boldsymbol{R}$*(*$\boldsymbol{R}$ *is the radius of circular cylinder), and the vortex shedding between the two cylinders maybe lead to sharp increasing of the force on the circular cylinder.*

Keywords: *Vortex Shedding, Force Suppression, Numerical Simulation, FFT*

1. Introduction

Flow around a cylinder has been widely studied due to its great importance in off shore practical engineering applications and fluid dynamics. The wake of a stationary circular cylinder in steady flow consists of two staggered rows of vortex when the Reynolds number exceeds about 47 (Williamson, 1996) [1]. The vortices shedding lead to a periodic force exerting on the circular cylinder, which generates the lift force has the same frequency as the vortex shedding cycle, and the frequency of drag equals twice of the shedding frequency. Many research works have done on the flow characteristics and hydrodynamic forces for flow past stationary circular cylinder (Williamson, 1989 [2]; Henderson, 1995 [3], 1997 [4]; Norberg, 2003 [5]; Baranyi and Lewis, 2006 [6]). The fluctuating lift is dominated by the actions from the periodic vortex shedding, which is the principal source of cross-stream flow-induced vibration. Vortex shedding will be dramatically changed when the cylinder oscillates in flow stream. Bishop and Hassan(1964) [7] investigated experimentally the hydrodynamic forces exerted on the cylinder in the cross-flow direction, and found that significant changed of the mean drag and the lift amplitude when the excitation frequency is close to the natural shedding frequency. Due to the alternate vortex shedding and consequently large amplitude lift fluctuations, vortex-induced vibrations (VIV) of cylindrical structures draw more and more attentions of engineers and researchers. Many methods have been proposed in order to suppress VIV responses(Lu, 2014) [8].

The method with smaller cylinders placing near the main cylinder as the control rods is an effective way to reduce the lift and suppress the VIV response if their arrangement is

ISSN: 2005-4297 IJCA
Copyright ⓒ 2015 SERSC

optimized(Lu, 2014)[8]. The problems of the steady flow passing two identical circular cylinders in tandem, side-by-side, and generally staggered arrangements have been extensively studied (Meneghini and Saltara, 2001 [9]; Cui *et al.*, 2014 [10]). For two cylinders in a tandem arrangement, Igarashi(1981) [11] conducted many experiments in a large range of Reynolds number and wide span of center-to-center distance. The results revealed that the fluid forces greatly depend on the Reynolds number and the spacing ratios. Sharman *et al.*, (2005) [12] carried out lots of numerical investigations at *Re*=100 and found the critical spacing of between 3.75 and 4.0 diameters, at which significant jumps in the fluctuating forces and the Strouhal number occur. If the gap ratio was small enough, the drag force on the downstream cylinder was found to be negative. Experiments of flow past two identical cylinders in a side-by-side arrangement was carried out, and results indicated that the vortex-shedding synchronization occurs either in phase or in antiphase as the gap between the cylinders exceeds a critical value (Williamson, 1985) [13]. The numerical results by Vakil and Green (2011) [14] shown that the flow patterns were significantly different from the case of an single cylinder even in very low Reynolds numbers for side-by-side arrangement cylinders. The wake interference leads to distinct variations in lift coefficient with spacing ratio, which is highly dependent on the Reynolds number. Zdravkovich (1968) [15] experimented laminar wake behind a three-cylinder group in various triangular configurations with low Reynolds number. Gu and Sun (2001) [16], Bao *et al.*, (2010) [17] conducted the numerical simulation for the flow past the three cylinders at low Reynolds number. Lu *et al.*, (2014)[8] investigated laminar flow past a circular cylinder with six small-diameter control rods. Four different flow regimes are identified based on the mechanism of lift and drag reduction. The results shown six-control-rod arrangement have better performance in flow control than the arrangements with less control rods, especially in terms of force reduction at various angles of attack.

The force suppression of setting triangular rod in the upstream of circular cylinder has not been studied in literatures. The structure of the paper is arranged as follows. The numerical model is briefly described in the next section followed some numerical verifications and validations. The numerical results are presented in Section 3, focusing on the influences of leg length of isosceles triangular rod, spacing ratio, vertex angle of the triangular rod on the vortex shedding and force coefficient. Finally, conclusions are drawn in Section 4.

2. Computational Model

2.1. Configuration and Computational Domain

The arrangement of an isosceles triangular rod being placed upstream the circular cylinder has been considered in uniform flow. A square computational domain is used for the numerical simulations of this arrangement. A sketch definition is presented in Figure 1.

 Copyright ⓒ 2015 SERSC

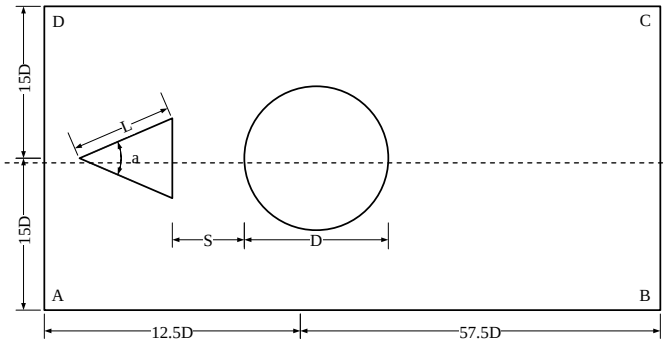

Figure 1. Computational Domain and Sketch Definition

A rectangular computational domain was adapted with a height of *30D* in the cross-flow direction and a width of *70D* in the flow direction. The *D* is the diameter of the circular cylinder, *L* is the length of legs of isosceles triangle, and *S* is the rod-to-cylinder spacing ratio from the base of isosceles triangular rod and edge of circular cylinder. The rectangular computational domain has same symmetry axis with isosceles triangular rod in horizontal.

The distance between the inlet boundary and the center of the stationary cylinder is *12.5D*. Edge AD in the computational is the inlet, where the first-type velocity boundary conditions of u=1 and v=*0*. At the outlet edge BC, the velocities are described as $\partial u_i/\partial t + c\partial u_i/\partial x = 0$, where c is the space-averaged exit velocity (Pauleyet al., 1990)[18]. The zero pressure $p = 0$ is adopted at the outflow boundary (Gresho and Sani, 1987)[19], whereas $\partial p/\partial n = 0$ is applied along the other boundaries, and n is the unit outward normal vector. Along the lateral boundaries, far from the cylinders, $\partial u/\partial y = 0$ and $v = 0$ are imposed. The no-slip boundary conditions of u=0 and v=*0* are imposed on the surfaces of the circular cylinder and the triangular rod.

Based on the surface integral along the circular cylinder, the drag coefficient and lift coefficient of the cylinder can be get by formula as(Zhou etal.,1999[20]; Baranyi, 2005[21]),

$$C_D(t) = F_x(t)/(\rho U^2 D/2), \quad (1)$$

$$C_L(t) = F_y(t)/(\rho U^2 D/2), \quad (2)$$

2.2. Configuration and Computational Mesh

It is well understood that the flow in the wake of a circular cylinder depends greatly on the Reynolds number defined by $Re = UD/v$, where U the flow velocity, and v is the kinematic viscosity.

The two-dimensional numerical models are employed to carry out simulations using a variety of parameters at low Reynolds number. The governing equations for simulating the flow are the two-dimensional incompressible Navier-Stokes (*N-S*) equations.

$$\frac{\partial u_i}{\partial x_i} = 0, \quad (3)$$

$$\frac{\partial u_i}{\partial t} + u_j \frac{\partial u_i}{\partial x_j} = -\frac{\partial p}{\partial x_i} + \frac{1}{\mathrm{Re}} \frac{\partial^2 u_i}{\partial x_j^2}, \quad (4)$$

Copyright ⓒ 2015 SERSC

where $x_1=x$ and $x_2=y$ are the Cartesian coordinates, $u_1 = u$ is the inline velocity and $u_2 = v$ is the cross-flow velocity, and p is the pressure.

2.3. Numerical Validations

The vortex shedding of an isolated stationary circular cylinder has been simulated to validate the simulation model in uniform flow. The results of lift coefficient and drag coefficient at the Reynolds number of *60, 80, 100, 150*, and *200* are shown in the Table 1 and Talble2 respectively.

Table 1. Drag Coefficients of Single Cylinder at Different Reynolds Number

Re	60	80	100	150	200
He(2000)[22]	1.39	1.35	1.35	---	1.36
Henderson(1995)[3]	1.42	1.37	1.35	1.33	1.34
Baiany(2006) [6]	1.41	1.36	1.34	1.33	---
Present	1.429	1.389	1.366	1.349	1.353

Table 2. Lift Coefficients of single Cylinder at Different Reynolds Number

Re	60	80	100	150	200
Farrant(2001)[23]	---	---	0.33	---	0.71
Zhang(2008) [24]	---	---	0.34	---	0.66
Baiany(2006) [6]	0.13	0.24	0.32	0.51	---
Present	0.12	0.23	0.32	0.50	0.64

Table 1 and Table 2 show that the results of the numerical model have good agreements between the present numerical results and those of the published literatures.

3. Numerical Results

3.1. Various of Forces Versus Leg Length and Distance at *Re=200* and $\alpha=60^o$

The nondimensional force of the circular is defined as $F_i=(F_{i\_max}-F_{i\_min})/2$ (i=x, y). The F_{x_max} and F_{x_min} are the maximum and the minimum drag force in the flow direction cylinder in not less than *80* periods of vibration. F_{y_min} and F_{y_min} are the maximum and the minimum lift force in the cross-flow direction.

In this section, the *Re* is *200* and the vertex angle is 60^o of the isosceles triangular cylinder. The aim is to find variation of force when the distance *S* changes from *0* to *10R*, and the leg length is in the range of *0.2R* and *0.7R*. Figure 2 presents forces variation versus leg length *L* and distance *S* at *Re=200* and $\alpha=60^o$.

 Copyright ⓒ 2015 SERSC

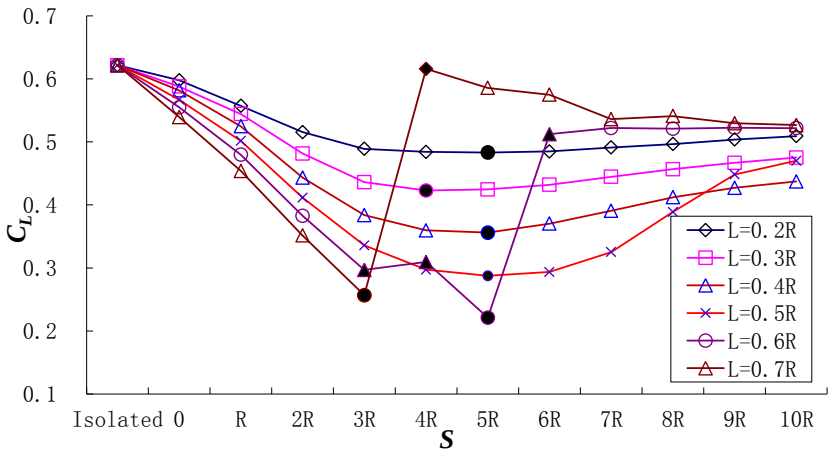

Figure 3. Lift Variation at *Re=200,* and $\alpha=60^o$

Figure 2 shows the arrangement of setting an equilateral triangular rod upstream the circular cylinder can take effective suppression of the lift in most cases. When L are 0.2R, 0.3R, 0.4R, 0.5R, 0.6R, and 0.7R, the most lift force reduction are 21.6%, 31%, 41.4%, 52.3%, 62.5%, and 56.9% with the appropriate distance S, respectively.

When *L* increases from *0.2R* to *0.5R*, the suppression of lift becomes more and more effective at the same distance *S*, except the cases of *S>0.9R* in *L=0.5R*. The suppression effect of lift enhances with the growing of *S* in the range of *S≤5R*, and drops with the growing of *S* when *S>5R* in the range of *0.2R≤L≤0.5R*.When *L=0.7R*, the lift drops with the growing of distance of triangular rod and circular cylinder if *S≤3R*. But if *S* increases to *4R*, the lift sharply jumps to 0.62 which is almost like the lift acting on the single cylinder without the triangular rod. For the case of *L=0.7R*, the analogue happens when *S* changes from *5R* to *6R*.

Figure 3 presents instantaneous vorticity contours for *S=5R* and *6R* at *L=0.6R*, *Re=200*, and $\alpha=60^o$.

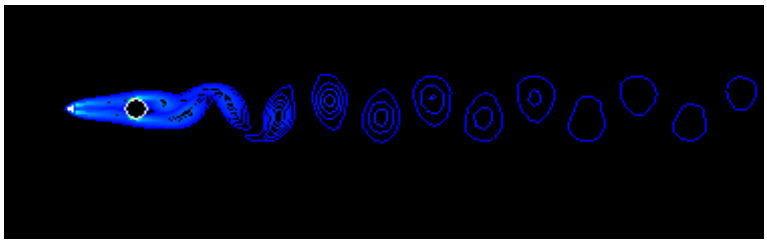

(a) S=5R

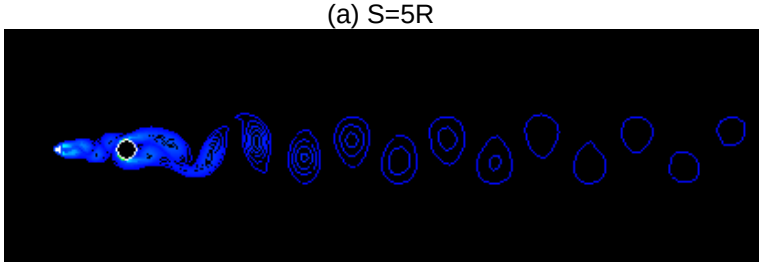

(b) S=6R

Figure 3. Instantaneous Vorticity Contours at *L=0.6R*.((a) *S=5R*, (b) *S=6R*)

Copyright ⓒ 2015 SERSC

The nondimensional vorticity is defined as $\omega = (\partial v / \partial x - \partial u / \partial y)/(U / D)$. In the Figure 3(a), the separated shear layers from the two legs of the isosceles triangular rod do not form vortices before they pass the circular cylinder. The circular cylinder is between the two shear layers from the two sides of the triangular rod. It can be seen that the circular cylinder delay the interaction between the shear layers from the two legs of the isosceles triangular rod. The interference of the circular cylinder on the vortex shedding from the triangular rod leads to the reduction of the force.

In the Figure3 (b), vortex shedding from the triangular rod occurs in the gap between the triangle and circular cylinders. After a vortex is separated from the triangular rod, it reaches the circular cylinder. The circular cylinder is trapped in the alternative negative and positive vortices from the triangular rod, which enhance the force not only in the streamwise but in the cross-flow direction.

Figure 4 is the time-history of lift for *S=5R* and *6R* at *L=0.6R*, *Re=200*, and $\alpha=60^o$.

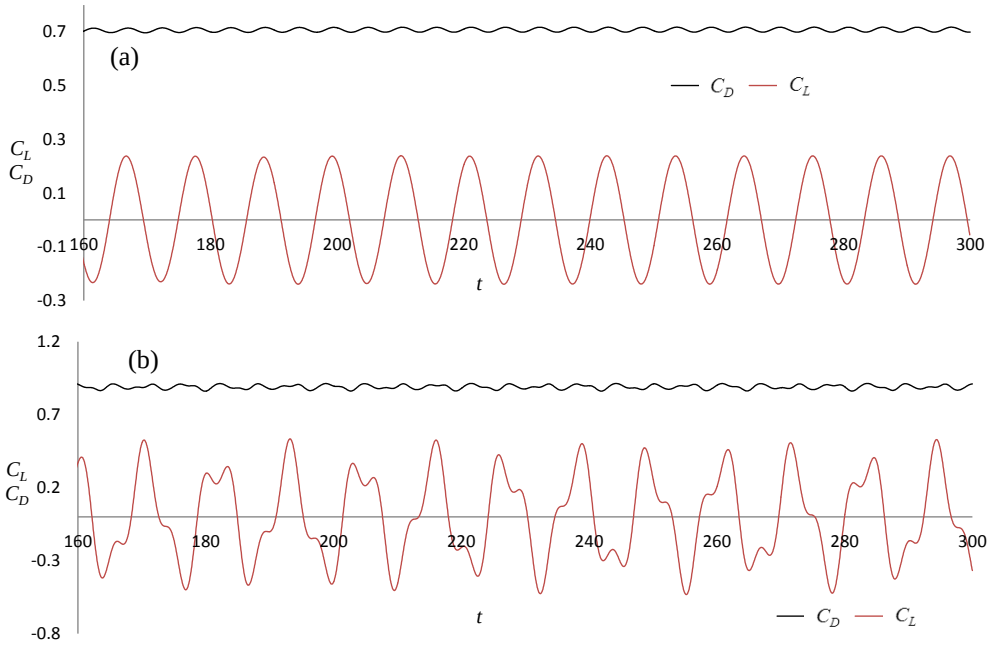

Figure 4. Time History of Force at *L=0.6R, Re=200, and*$\alpha=60^o$. ((a) *S=5R,* (b) *S=6R*)

Figure 4 shows that the lift on the circular changes regularly with a single dominate frequency at *S=5R*, but irregularly with multiple frequencies at *S=6R*. This is in accordance with the vortex shedding shown in Figure 3. The fast Fourier transform (FFT) has been used to determine frequency components of lift and Drag. Figure 5(a) and (b) are the spectra of lift and drag for *S=5R* and *6R.*

Copyright ⓒ 2015 SERSC

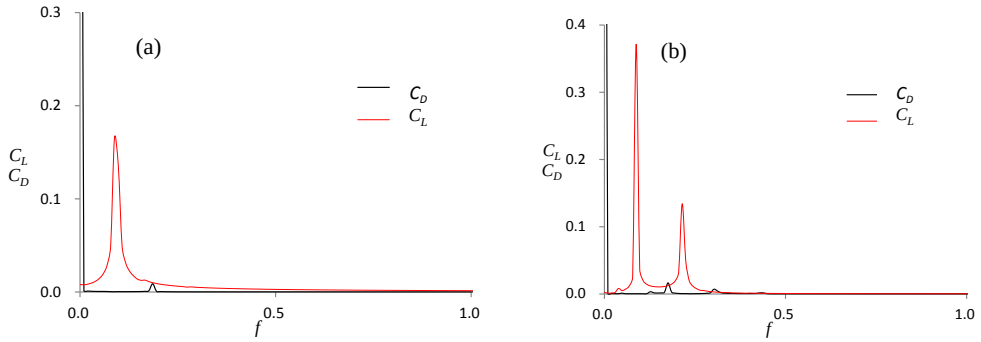

Figure 5. Spectra of Lift and Drag for S=5R and 6R at L=0.6R, Re=200, and α=60°. ((a) S=5R, (b) S=6R)

Figure 6 is the drag various at *L=0.6R*, *Re=200*, and *α=60°*. The arrangement of the triangular rod in the upstream of the circular cylinder can also reduce the drag effectively in the suitable situation.

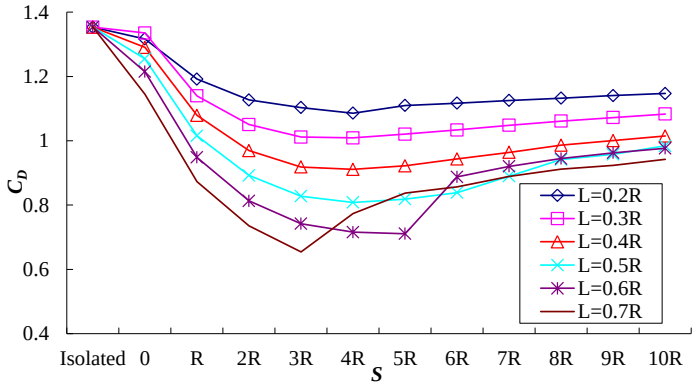

Figure 6. Drag Variation at *L=0.6R*, *Re=200*, and *α=60°*

It can be seen from this section, in the ranges of $0.2R \leq L \leq 0.5R$ and $3R \leq S \leq 6R$ with $\alpha = 60^{o}$, the arrangement of setting equilateral triangular rod in the upstream of the circular cylinder can take effective suppression on not only the lift but also the drag.

Based on these results, the next section focuses on the effect of vertex angle of the isosceles triangular α and rod-to-cylinder spacing ratio S at $L=0.4R$ and $Re=200$.

3.2. Various of Forces Versus Vertex Angle α and Distance *S* at *Re=200* and *L=0.4R*

Figure 7 presents lift variation versus vortex angle$\alpha$and distance S at $Re=200$ and $L=0.4R$.

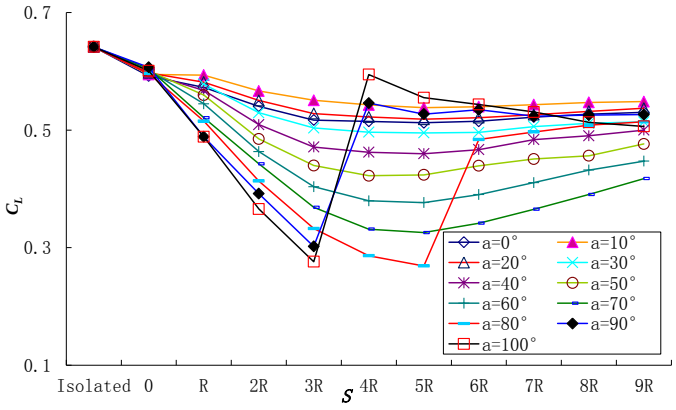

Figure 7. Lift Variation at *L=0.4R, Re=200*

When $a \leq 70^o$, the suppression of lift becomes more and more effective with the increasing of S in the range of $S \leq 5R$. But if $S>5R$, the suppression decreases with the increasing of S. When a increases from 10^o to 70^o, the suppression of lift becomes more and more effective at the same value of S. For the case of $a = 0^o$, the effect for lift suppression is better than the case of $a = 20^o$, and is worse than the case of $a=30^o$. For the same vertex angle a , the suppression of lift enhances with the growing of S when $S \leq 4R$, and drops with the growing of S when $S>4R$ in the range of $0 \leq a \leq 70^o$.

When $a=80^o$, the lift drops with the growing of distance S in the range of $S \leq 5R$. But if S increases to $6R$, the lift sharply jumps to 0.484. Time history of lift for $S=5R$ and $6R$ are shown in Figure 8 at $Re=200$, $L=0.4R$, and $a=80^o$.

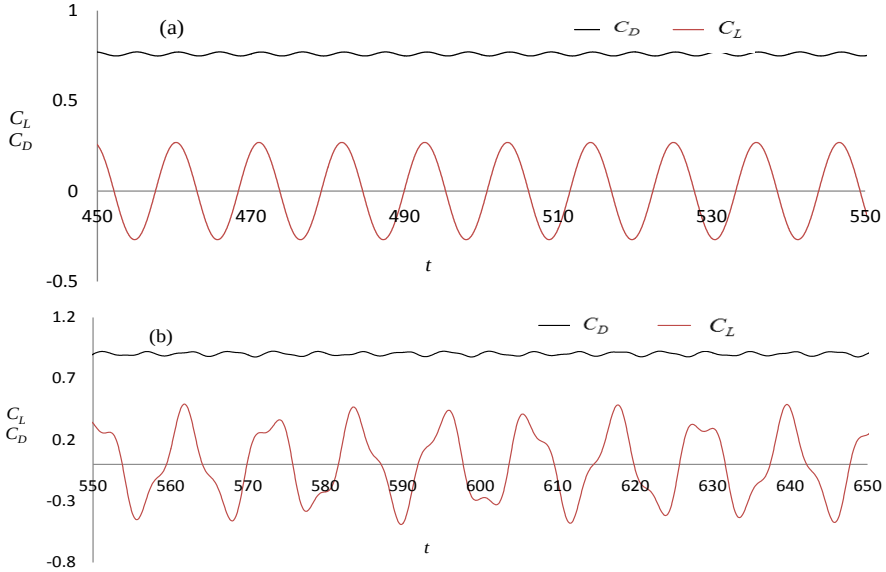

Figure 8. Time History of Force at *Re=200, L=0.4R*, and *a=80°*.((a) *S=5R*, (b) *S=6R*)

Copyright ⓒ 2015 SERSC

The phenomena in Figure 8 is very similar to the time history of lift for *S=5R* and *6R* at *L=0.6R, Re=200,* and $\alpha=60^o$.

For the case of $\alpha=90^o$ and 100^o, the same thing happens when *S* increases from *3R* to *4R*. Figure 9 is the variation of drag at *L=0.6R, Re=200,* and $\alpha=60^o$.

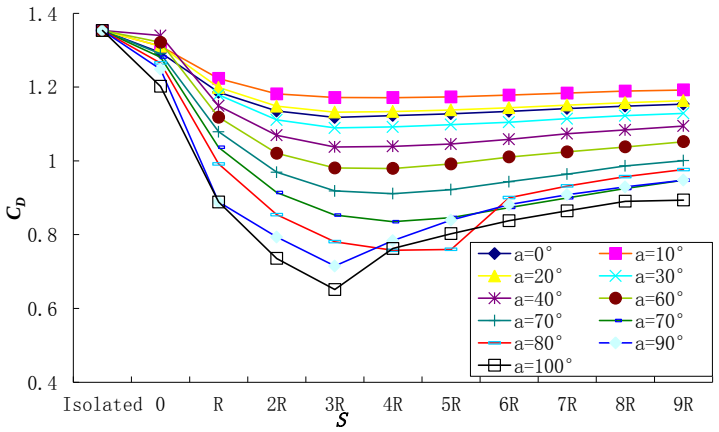

Figure 9. Drag Variation at *Re=200, L=0.4R*

Figure 9 shows that the suppression of drag is similar to that of lift, when vertex angle α is between the 0^o and 70^o. The difference is the minimum value for lift at about *S=4R* but for drag at about *S=5R*.

3.3. Various of Forces versus *Re* and *S* at $\alpha=60^o$ and *L=0.4R*

Figure 10 presents lift and drag variation with the *Re* and *S* at $\alpha=60^o$ and *L=0.4R* with a larger range of rod-to-cylinder spacing ratio *S*. When the spacing ratio *S* is between *0* and *20D*, $3R \leq S \leq 6R$ is the more effective range for the force suppression of setting a triangular rod upstream the cylinder.

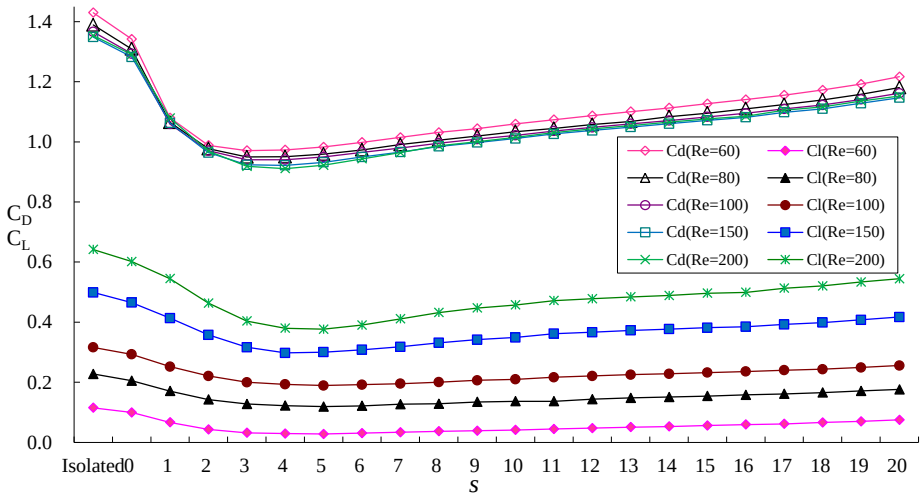

Figure 10. Lift and Drag Variation for the Triangular Nod with *L=0.4R*, and *a=60^o* at *Re=60, 80, 100, 150,* and *200*

Copyright ⓒ 2015 SERSC

4. Conclusion

The arrangement of an isosceles triangular rod in the upstream to suppress the force on the circular cylinder was simulated numerically at *Re=200, 100, 150, 100, 80,* and *60.* Navier-Stokes (*N-S*) equations are solved numerically for predicting the lift and the drag acting on the circular cylinder, respectively.

The results indicate that the arrangement of setting the equilateral triangular rod in the upstream of the circular cylinder can take effective suppression of not only the lift but the drag in the range of $0.2R \leq L \leq 0.5R$ and $3R \leq S \leq 6R$.

Acknowledgment

The authors would like to acknowledge the support from National Natural Science Foundation of China (Grant No.61272021, 51179174), the China Spark Program(Grant No.2012GA700193, 2013GA700258), and the Open Foundation from Marine Sciences in the Most Important Subjects of Zhejiang (Grant No.20140101).

References

[1] C. H.K. Williamson. Vortex dynamics in the cylinder wake. Annu Rev Fluid Mech. 28 **(1996)**.
[2] C. H. K. Williamson. Oblique and parallel modes of vortex shedding in the wake of a circular cylinder at low Reynolds number. Journal of Fluid Mechanics.10, 206**(1989).**
[3] R. D. Henderson. Details of the drag curve near the onset of vortex shedding. Physics of Fluids.7,2102**(1995)**.
[4] R. D. Henderson. Nonlinear dynamics and pattern formation in turbulent wake transition. Journal of Fluid Mechanics.12, 352**(1997)**.
[5] C. Norberg, Fluctuating lift on a circular cylinder: review and new measurements. Journal of Fluids and Structures.1,17**(2003).**
[6] L. Baranyi and R.I. Lewis. Comparison of a grid-based CFD method and vortex dynamics predictions of low Reynolds number cylinder flows. Aeronautical Journal.1, 110**(2006).**
[7] R. E. D. Bishop and A. Y. Hassan. The Lift and Drag Forces on a Circular Cylinder Oscillating in a Flowing Fluid. Proceedings of the Royal Society A: Mathematical, Physical and Engineering Sciences. 1368, 277**(1964)**.
[8] L. Lu, M.M. Liu, B. Teng and Z.D. Cui. Numerical investigation of fluid flow past circular cylinder with multiple control rods at low Reynolds number. Journal of Fluids and Structures.7, 48**(2014)**.
[9] J. R. Meneghini and F. Saltara. Numerical simulation of flow interference between two circular cylinders in tandem and side-by-side arrangements. Journal of Fluids and Structures.2, 15**(2001)**.
[10] Z. D. Cui, M. Zhao and B. Teng. Vortex-induced vibration of two elastically coupled cylinders in side-by-side arrangement. Journal of Fluids and Structures. 1,44**(2014)**.
[11] T. Igarashi. Characteristics of the flow around two circular cylinders arranged in tandem. Bulletin of JSME.2, 24**(1981).**
[12] B. Sharman, F. S. Lien, L. Davidson and C. Norberg. Numerical predictions of low Reynolds number flows over two tandem circular cylinders. International Journal for Numerical Method in Fluids.2, 47**(2005)**.
[13] C. H. K. Williamson. Evolution of a single wake behind a pair of bluff bodies. Journal of Fluid Mechanics .9,159**(1985).**
[14] A. Vakil and S.I. Green. Two-dimensional side-by-side circular cylinders at moderate Reynolds numbers. Computers and Fluids.1, 51**(2011).**
[15] M. M. Zdravkovich. Smoke observations of the wake of a group of three cylinders at low Reynolds number. Journal of Fluid Mechanics.2, 32**(1968)**.
[16] Z. F. Gu and T.F. Sun. Classifications of flow pattern on three circular cylinders in equilateral-triangular arrangements. Journal of Wind Engineering and Industrial Aerodynamics. 6, 89(**2001**).
[17] Y. Bao, D. Zhou and C. Huang. Numerical simulation of flow over three circular cylinders in equilateral arrangements at low Reynolds number by a second-order characteristic-based split finite element method. Computers and Fluids.5,39**(2010)**.
[18] L. L. Pauley, P. Moin and W.C. Reynolds. The structure of two-dimensional separation. Journal of Fluid Mechanics. 12,220 **(1990)**.
[19] P. M. Gresho and R. L. Sani. On pressure boundary conditions for the incompressible Navier–Stokes equations. International Journal for Numerical Method in Fluids.10,7,**(1987)**.

 Copyright ⓒ 2015 SERSC

[20] C. Y. Zhou, R. M. C So and K. Lam. Vortex-induced vibrations of an elastic circular cylinder. Journal of Fluids and Structures. 2, 13**(1999)**.
[21] L. Baranyi. Lift and drag evaluation in translating and rotating non-inertial systems. Journal of Fluids and Structures.1, 20**(2005)**.
[22] J. W. He, R. Glowinski, R. Metcalfe, A. Nordlander and J. Periaux. Active control and drag optimization for flow past a circular cylinder I. oscillatory cylinder rotation, J. Comput. Phys. 163, 83**(2000)**.
[23] T. Farrant, M. Tan and W. G. Price. A cell boundary element method applied to laminar vortex shedding from circular cylinders, Comput. Fluids. 30, 211 **(2001).**
[24] X. Zhang, S. Z. Ni and G.W. He. A pressure-correction method and its applications on an unstructured Chimera grid, Comput. Fluids. 37, 993 **(2008).**

Author

Zhendong Cui, he is an Associate Professor at Zhejiang Ocean University in China. He received the P.h.D. degree from Dalian University of Technology in June, 2008. His main research interests include science and engineering computing and distributed computing.

Copyright ⓒ 2015 SERSC